Supporting Information For:

Insights into Molecular Magnetism in Metal-Metal Bonded Systems as Revealed by a Spectroscopic and Computational Analysis of Diiron Complexes

Samuel M. Greer[a,b], *Kathryn M. Gramigna*[c], *Christine M. Thomas*[e,*], *Sebastian A. Stoian*[d,*], *Stephen Hill*[a,f,*]

[a] National High Magnetic Field Laboratory, Florida State University, Tallahassee, FL 32310, USA.

[b] Department of Chemistry and Biochemistry, Florida State University, Tallahassee, FL 32306, USA.

[c] Department of Chemistry, Brandeis University, Waltham, MA 02453, USA.

[d] Department of Chemistry, University of Idaho, Moscow, ID 83844, USA

[e] Department of Chemistry and Biochemistry, The Ohio State University, Columbus, OH 43210, USA.

[f] Department of Physics, Florida State University, Tallahassee, FL 32306, USA.

[*] Corresponding authors E-mail: thomasc@chemistry.ohio-state.edu, sstoian@uidaho.edu, and shill@magnet.fsu.edu

Table of Contents

High Field EPR Spectra (HFEPR)

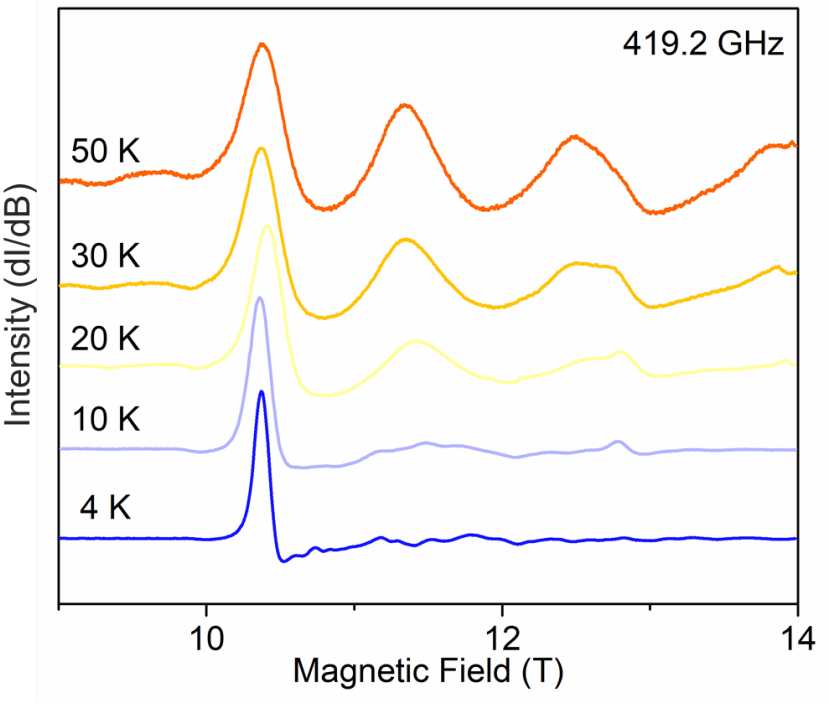

Figure S1. Variable temperature EPR spectra of **2** recorded at 419.2 GHz.

As described in the main text, the variable-frequency HFEPR spectra of **2** were recorded 30 K. We chose this temperature to both avoid the unusual features observed at lower temperatures as well as to see the maximum number of transitions with reasonable resolution. Our goal was to definitively assign ground state zero field splitting (ZFS) parameters and look for evidence for higher order parameters.

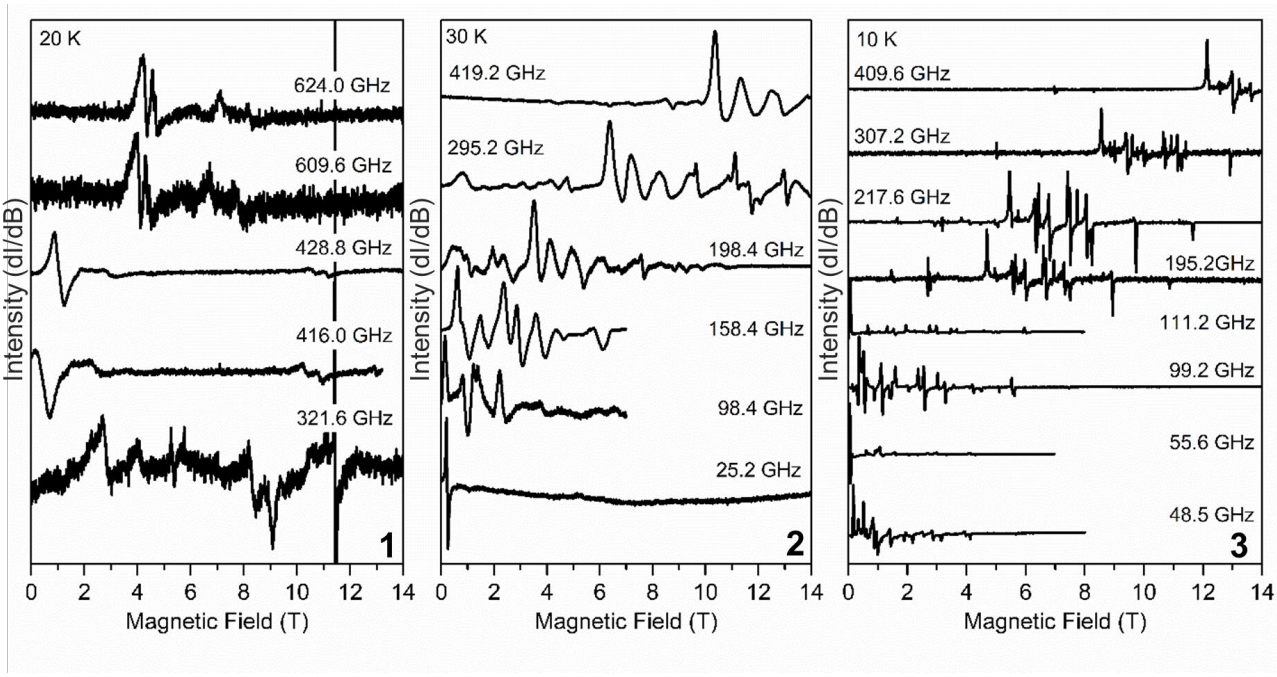

Figure S2. Series of HFEPR spectra used for the evaluation of *D*, *E*, and the *g*-factors for **1-3.**

Mössbauer Spectra and Analysis

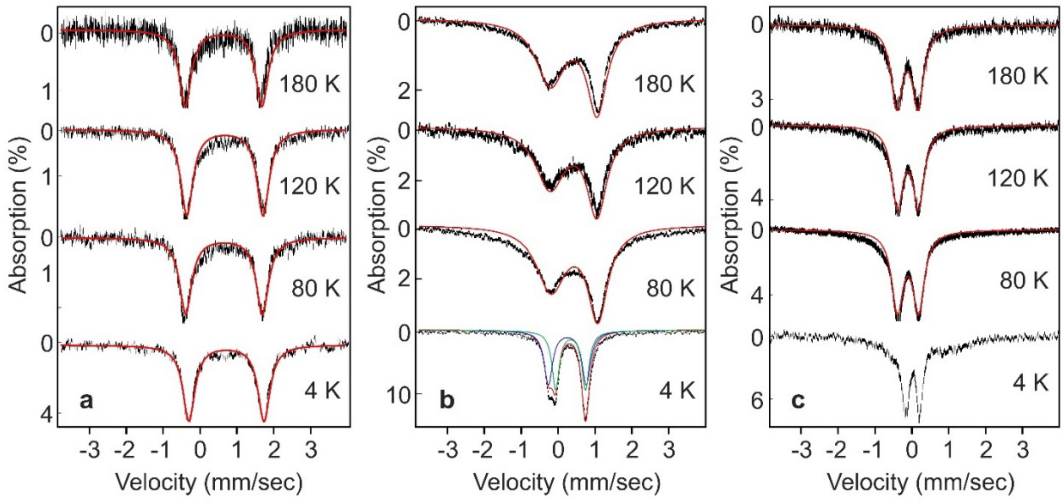

Figure S3. Variable temperature ^{57}Fe Mössbauer spectra of **1** (a), **2** (b) and **3** (c).

Table S1. Variable Temperature Mössbauer Parameters of **1**, **2**, and **3**.

	1		**2**		**3**	
Temp. (K)	ΔE_Q (mm/s)	δ (mm/s)	ΔE_Q (mm/s)	δ (mm/s)	ΔE_Q (mm/s)	δ (mm/s)
180	2.05	0.62	1.27	0.42	0.58	-0.09
120	2.08	0.65	1.23	0.42	0.57	-0.08
80	2.10	0.66	1.25	0.43	0.57	-0.07
4	-2.05	0.66	-1.11/1.41	0.56/0.44	0.51/-*	-0.04/-*

*See main text

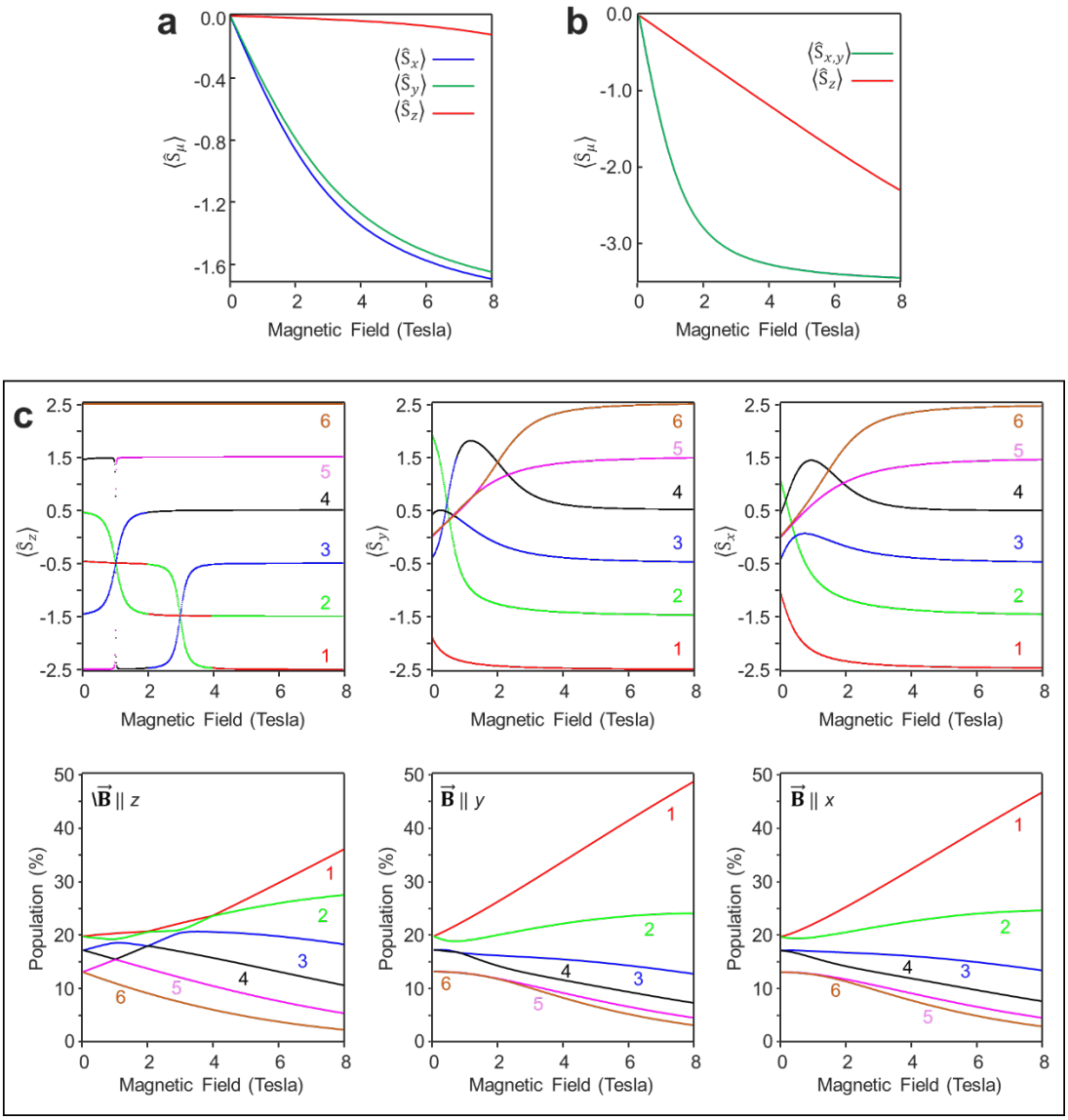

Figure S4. Thermally averaged spin expectation values calculated using the HFEPR derived spin Hamiltonian parameters for **1** (a) and **2** (b) at 4.2 K, and plotted as function of the applied field. The magnetic field is applied along the *x* (green), *y* (blue) and *z* (red) components of the ZFS tensors. (c) Spin expectation values for each sublevel of the ground spin state in **3** (top row). The Boltzmann population of each spin sublevel as a function of magnetic field (bottom row). The number corresponds to the energetic ordering of each level such that the energy of the level increases from 1-6.

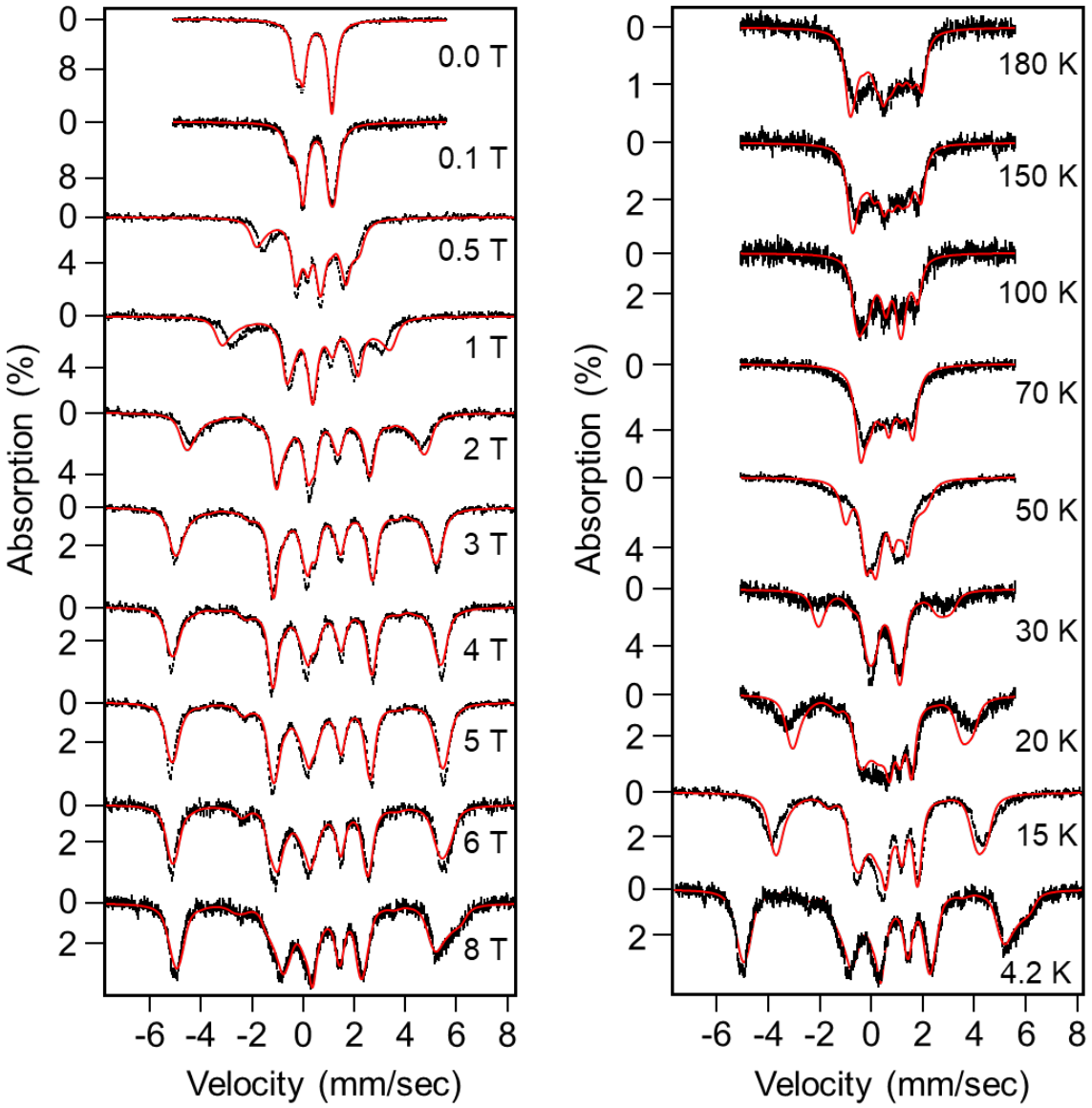

Figure S5. Experimental (black) and simulated (red) ^{57}Fe Mössbauer spectra at varying applied fields and temperatures for **2.**

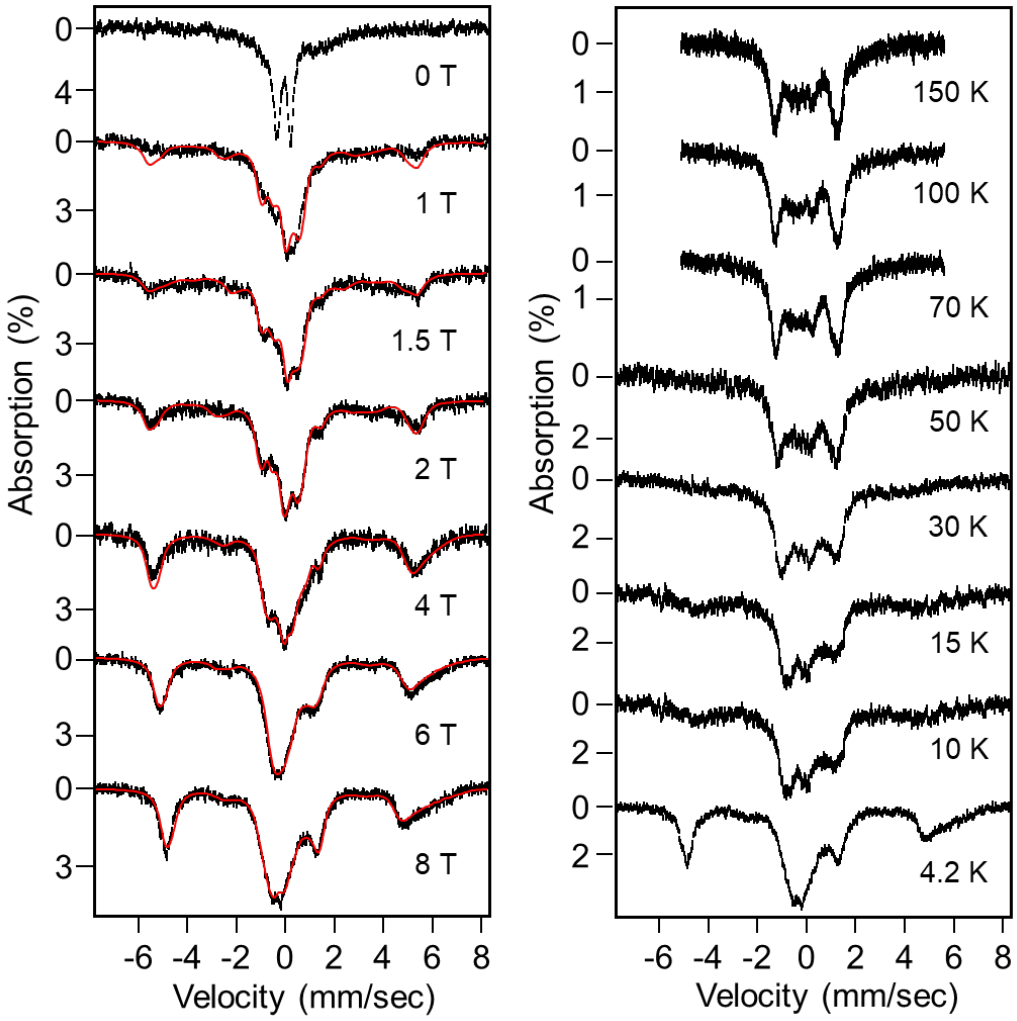

Figure S6. Experimental (black) and simulated (red) ^{57}Fe Mössbauer spectra at varying applied fields and temperatures for **3.** Due to relaxation effects only the low temperature data is simulated.

Ground State Complete Active Space Self-Consistent Field (CASSCF) Calculations

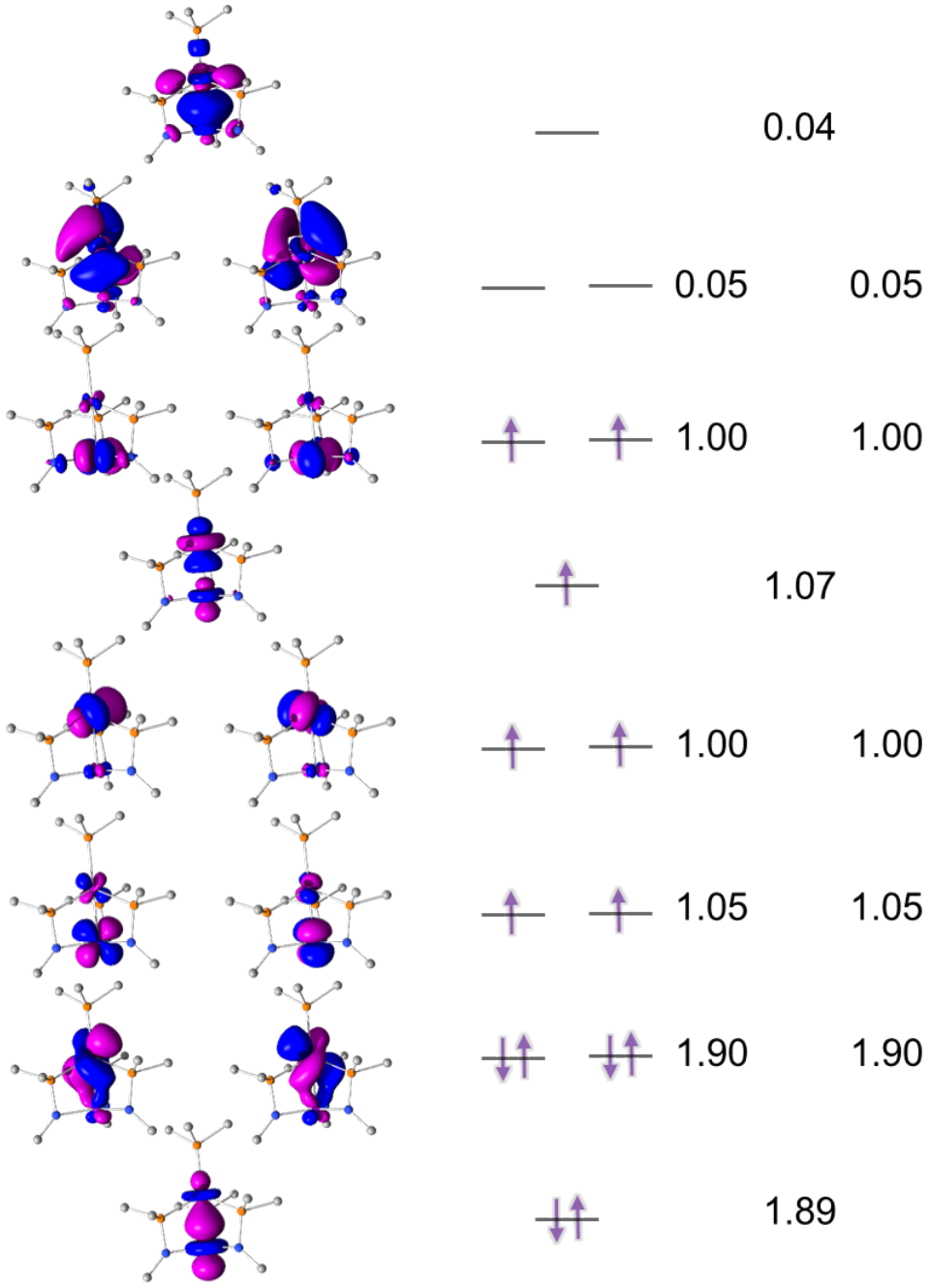

Figure S7. Qualitative MO diagram for **2** showing the results of the CAS(13,13) orbitals. Here the extra three (mostly) virtual orbitals correspond to 4d orbitals. We chose to include these to make the calculation consistent with those reported in ref 23 by Zall *et. al*. The dominant configuration (~83%) is shown. The numbers to the right indicate the populations of each orbital.

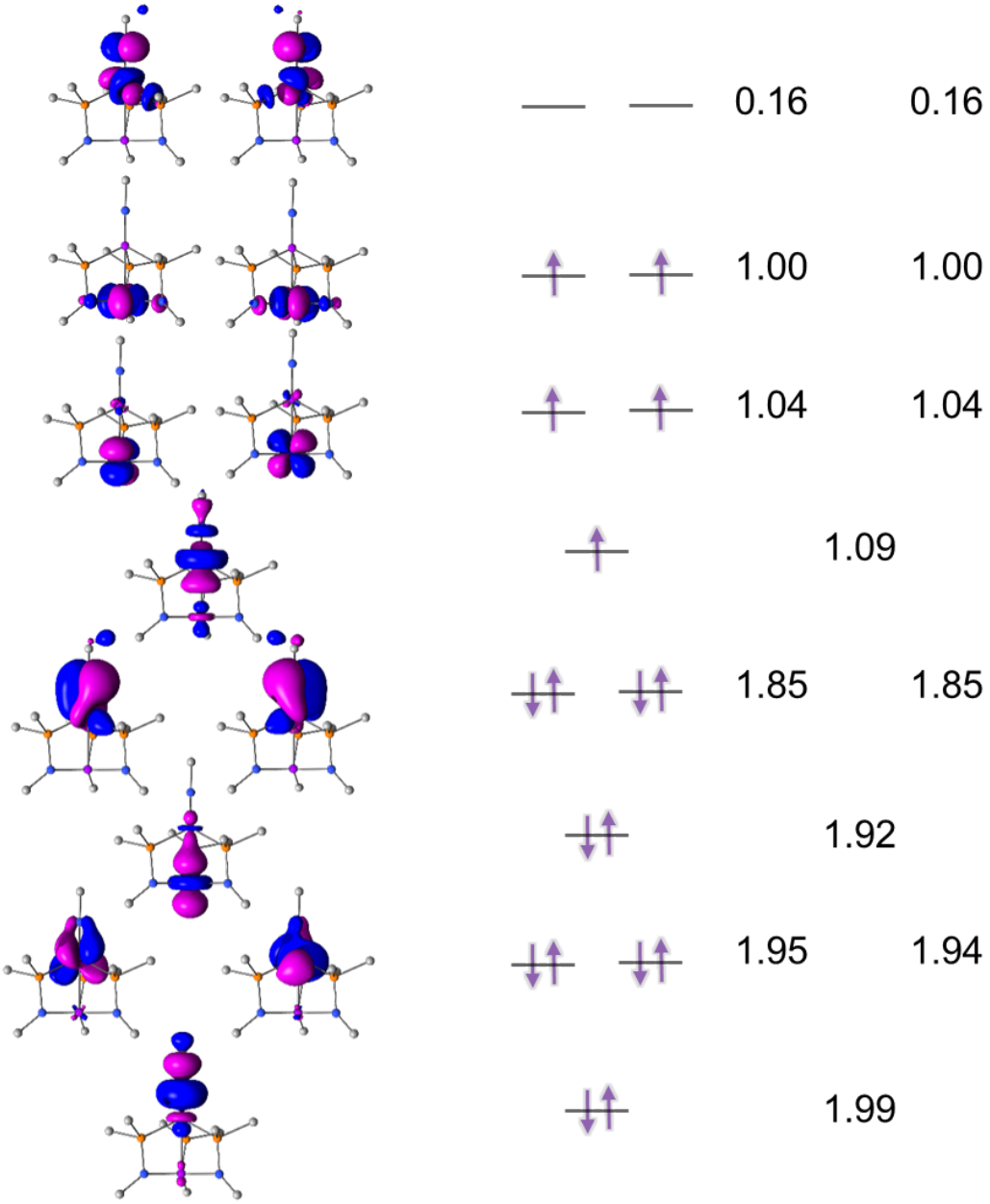

Figure S8. Qualitative MO diagram for **3** showing the results of the CAS(17,13) orbitals. Here the extra three virtual orbitals correspond to 4d orbitals. The dominant configuration (~77%) is shown. The numbers to the right indicate the populations of each orbital. To facilitate comparison with our qualitative MO diagrams in the main text this calculation was performed on a fully optimized and, thus, higher symmetry model of **3**.

Density Functional Theory (DFT) Calculation of Mössbauer Parameters

To determine the relative ligand and valance contributions to the electric field gradient (EFG), we have performed calculations for **1** and a theoretical analogue in which the Fe(II) site is replaced by Zn(II). Here, the Zn(II) analogue will have no valance contribution and, therefore, the entire EFG is generated by the ligands. The ligand contribution can then be subtracted from the total to reveal the valance contribution. The results of this calculation are shown in Table S2 and confirm that the asymmetry of the EFG originates from the valance contribution. We also compare the calculated parameters of **1** using B3LYP and BP86. Here we find that the largest difference is in the magnitude of the fermi contact contribution to the hyperfine coupling. The BP86 functional predicts a value of A_{fc} ~$^2/_3$ that predicted by B3LYP. The magnitude of the quadrupole splitting is 0.18 mm/sec larger using BP86 and the isomer shift is 0.02 mm/sec larger in BP86 than in B3LYP.

Table S2. DFT-Mössbauer and ZFS Parameters for **1** – **3** at the BP86/CP(PPP)(Fe), def2-tzvp(P/N), and def2-svp(C/H) level of theory (x-ray structures).

	S	δ (mm/s)	ΔE_Q (mm/s)	η	A_{iso} (MHz)	D (cm^{-1})	E/D
1	2	0.50	-2.45	0.75	-8.57	2.86	0.09
^{P}**2**	$^7/_2$	0.42	-1.10	0.01	-3.88	0.48	0.01
^{N}**2**		0.36	1.21	0.01	-9.44		
^{P}**3**	$^5/_2$	-0.15	0.47	0.20	-1.81	0.07	0.31
^{N}**3**		0.34	1.68	0.05	-9.28		

Table S3: Calculated Mossbauer Parameters for **1** (B3LYP, x-ray structure)

	ΔE_Q(mm/s)	δ (mm/s)	η	A_i	A_x (MHz)	A_y(MHz)	A_z(MHz)
1	-2.27	0.48	0.80	A_{fc}	-15.52	-15.52	-15.52
				A_{dip}	7.09	2.54	-9.63
				A_L	5.04	4.84	-0.36
				A_{Tot}	-3.40	-8.14	-25.51

Table S4. DFT Calculated contributions to the ^{57}Fe $\tilde{\mathbf{A}}$-tensors for **1**, **2**, and **3** at the BP86/ CP(PPP)(Fe), def2-tzvp(P/N), and def2-svp(C/H) level of theory (x-ray structures).

		N-Site (MHz)			P-Site (MHz)		
		A_x	A_y	A_z	A_x	A_y	A_z
1	A_{fc}	-10.56	-10.56	-10.56			
	A_{dip}	6.57	1.65	-8.22			
	A_L	3.23	2.94	-0.21			
	A_{tot}	-0.76	-5.97	-18.99			
2	A_{fc}	-9.94	-9.94	-9.94	-4.84	-4.84	-4.84
	A_{dip}	1.05	1.05	-2.10	0.84	0.84	-1.68
	A_L	0.75	0.75	-0.01	0.97	0.97	0.96
	A_{tot}	-8.14	-8.14	-12.05	-3.03	-3.04	-5.56
3	A_{fc}	-9.89	-9.89	-9.89	-1.94	-1.94	-1.94
	A_{dip}	0.99	0.77	-1.76	-1.07	-1.32	2.39
	A_L	0.72	0.72	0.32	0.05	0.03	0.30
	A_{tot}	-8.15	-8.37	-11.33	-2.96	-3.23	0.76

Table S5. DFT predicted reduced Mulliken orbital charges and spins for **1**, **2**, and **3** at the BP86/ CP(PPP)(Fe), def2-tzvp(P/N), and def2-svp(C/H) level of theory (x-ray structures).

	1		**2**				**3**			
			P		**N**		**P**		**N**	
	charge	*spin*	*charge*	*spin*	*charge*	*spin*	*charge*	*spin*	*charge*	*spin*
s	6.36	0.04	6.39	0.18	6.52	0.05	6.51	0.03	6.46	0.11
p_z	4.23	0.03	4.32	0.00	4.45	0.06	4.53	0.01	4.38	0.09
p_x	4.36	0.03	4.32	0.16	4.25	0.03	4.40	0.01	4.23	0.04
p_y	4.35	0.05	4.32	0.16	4.25	0.03	4.40	0.02	4.25	0.04
d_{z2}	1.28	0.62	1.32	0.45	1.44	0.43	1.35	0.22	1.34	0.54
d_{xz}	1.44	0.50	1.34	0.45	1.16	0.79	1.07	0.11	1.17	0.77
d_{yz}	1.13	0.82	1.34	0.44	1.16	0.79	1.08	0.12	1.17	0.77
d_{x2-y2}	1.22	0.76	1.25	0.55	1.22	0.74	1.49	0.09	1.24	0.71
d_{xy}	1.23	0.75	1.25	0.55	1.22	0.74	1.50	0.08	1.24	0.72

Table S6. Evaluation of the DFT calculated EFG (a.u.$^{-3}$) in **1** at the BP86/CP(PPP)(Fe), def2-tzvp(P/N), and def2-svp(C/H) level of theory

Model	**Contrib.**	**Tensor Components**						**Principal Values**			ΔE_Q [mm/s]	η
		xx	*yy*	*zz*	*xy*	*xz*	*yz*	*min*	*mid*	*max*		
$[Fe(NH_2)_3]^{1-}$	lig.	-1.269	-1.297	2.566	0.048	0.301	0.182	-1.265	-1.334	2.598	4.21	0.03
	val.	0.696	0.759	-1.456	-0.052	-0.103	-0.081	0.674	0.788	-1.464	-2.37	0.08
	tot.	-0.572	-0.538	1.110	-0.004	0.198	0.101	-0.540	-0.599	1.139	1.84	0.05
$[Fe(HNPH_2)_3]^{1-}$	lig.	-1.047	-1.052	2.098	0.027	0.294	0.149	-1.051	-1.082	2.133	3.46	0.01
	val.	0.732	0.872	-1.604	-0.031	0.231	0.080	0.750	0.879	-1.629	-2.64	0.08
	tot.	-0.315	-0.179	0.495	-0.004	0.525	0.229	-0.195	-0.601	0.795	1.34	0.51
$FeCu_2(NHPH_2)_4$	lig.	-1.014	-1.045	2.058	0.037	0.277	0.146	-1.021	-1.069	2.090	3.39	0.02
	val.	0.526	0.933	-1.458	-0.154	0.462	0.221	0.599	0.987	-1.585	-2.59	0.24
	tot.	-0.488	-0.112	0.600	-0.117	0.739	0.367	-0.088	-0.953	1.041	1.87	0.83
x-ray	lig.	-0.957	-0.975	1.931	-0.061	-0.319	0.342	-0.977	-1.030	2.006	3.25	0.03
	val.	-0.073	0.921	-0.846	0.584	0.818	-0.588	0.409	1.216	-1.623	-2.74	0.50
	tot.	-1.030	-0.054	1.085	0.523	0.499	-0.246	0.172	1.211	-1.383	-2.45	0.75

Table S7. Diagnostic structural metrics for comparison of **1**, ^{N}**2**, and ^{N}**3.**

Metric	1	^{N}2	^{N}3
Fe-N distance (Å)	1.999, 1.976, 1.983	1.946, 1.946, 1.940	1.967, 1.966, 1.965
N-Fe-N angle (˚)	122.47, 121.4, 115.95	121.45, 119.71, 118.84	119.99, 119.96, 120.04
P-N-Fe-N dihedral (˚)	84.01, 77.89, 74.16	82.80, 82.12, 81.17	78.34, 78.34, 78.34
Fe-N-P angle (˚)	118.75, 103.78, 103.33	93.12, 92.88, 92.32	95.91, 95.91, 95.90
Fe-N-C angle (˚)	123.72, 132.69, 135.00	137.06, 138.57, 137.69	136.29, 136.29, 136.29

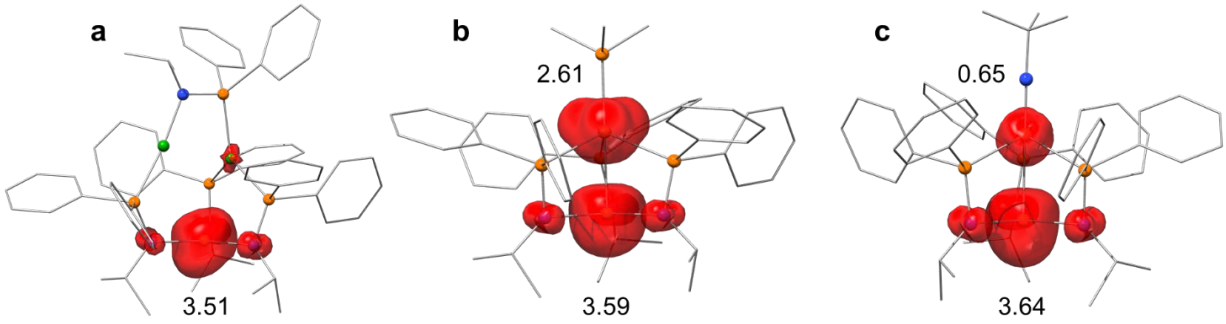

Figure S9. DFT calculated spin density distributions and Löwdin spin populations for **1** (a), **2** (b), and **3** (c).

ZFS Perturbation Theory Expressions

Using Eq. 4 (main text) we find that the spin-orbit coupling in **1** is essentially quenched along *z* but induces sizable mixing along *x* and *y*. Following the standard procedure, we can derive expressions for the ZFS parameters and *g*-factors:

$$g_z = g_e\,; \qquad g_y = g_e + \frac{3k^2\zeta}{2\Delta_{xz}}\,; \qquad g_x = g_e + \frac{3k^2\zeta}{2\Delta_{yz}} \tag{S1}$$

$$D = \frac{3}{32}\zeta^2\left(\frac{k^2}{\Delta_{yz}} + \frac{k^2}{\Delta_{xz}}\right);\; E = \frac{3}{32}\zeta^2\left(\frac{k^2}{\Delta_{xz}} - \frac{k^2}{\Delta_{yz}}\right). \tag{S2}$$

Here, g_e is the free electron g-value and k is the orbital reduction factor.

Ligand Field Theory (LFT) Calculations for **1**

To model the effects of triplet states on the magnitude of D, we have performed a series of LFT calculations where we have varied the size of the electron repulsion parameters B and C while keeping a fixed ratio of $B/C = 4.3$. We create the ligand field potential using the angular overlap model (AOM) which parameterizes the σ and π bonding of the coordinated ligands. In a planar C_3 symmetric molecule the energies (E) of the d-orbitals are found to be:

$$E(d_{z2}) = \frac{3}{4}e_\sigma$$

$$E(d_{yz}) = E(d_{xz}) = \frac{3}{2}e_{\pi c}$$

$$E(d_{xy}) = E(d_{x2\text{-}y2}) = \frac{9}{8}e_\sigma + \frac{3}{2}e_{\pi s}$$

Within this framework we have chosen a set of bonding parameters which reproduce the observed splittings, $e_\sigma = 28000$ cm^{-1}, $e_{\pi c} = 16000$ cm^{-1}, and $e_{\pi s} = 0$. The result of this series of calculations is shown in Figure S10. The vertical red line indicates the free ion value of B for Fe(II). At this value the contributions of the triplet states to D is 2.1 cm^{-1}, in fair agreement with our experimental results.

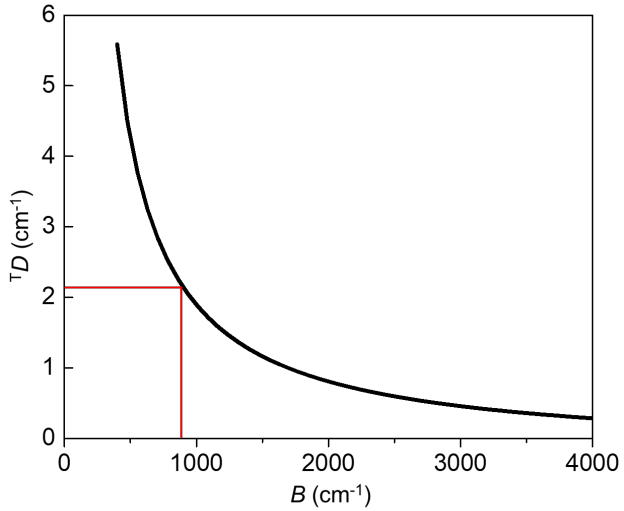

Figure S10. Plot showing the effect of triplet states on the magnitude of D in a trigonal planar coordination environment. The red line indicates the free ion value for Fe(II) and the corresponding triplet state contribution. Calculated with $\zeta = 427$ cm^{-1}.

CASSCF/NEVPT2 Calculations

Table S8. CASSCF/NEVPT2 calculated excited states and contributions^ to *D* in **2**.*

Excited State	CASSCF		NEVPT2	
	Energy (cm^{-1})	*D* (cm^{-1})	Energy (cm^{-1})	*D* (cm^{-1})
$^8E(\sigma\rightarrow\pi^*)$	2423	+2.44	4110	+1.46
$^8E(\sigma\rightarrow\pi^*)$	2427	+2.44	4112	+1.46
$^8A_1(\pi\rightarrow\pi^*)$	4701	-0.11	6615	-0.08
$^8E(\pi\rightarrow\sigma^*)$	4760	+1.47	6924	+1.02
$^8E(\pi\rightarrow\sigma^*)$	4763	+1.46	6927	+1.01
$^8A_1(\pi\rightarrow 2e_P)$	5425	-1.31	7151	-0.99
$^6E(\sigma\rightarrow\pi^*)$	1236	-0.30	2139	-0.17
$^6E(\sigma\rightarrow\pi^*)$	1240	-0.30	2142	-0.17
$^6E(\pi\rightarrow\sigma^*)$	4951	-0.16	7230	-0.11
$^6E(\pi\rightarrow\sigma^*)$	4954	-0.16	7234	-0.11
$^6A_1(\pi\rightarrow 2e_P)$	6030	+0.32	8120	+0.23
Total		+5.32		+3.42

^Only states with a contribution to the ZFS larger than 1% of the total value are shown.

*The listed values come from a SA-CAS(10,11) with 10 roots of both multiplicity 6 and 8.

Table S9. Comparison of calculated *D* values for **2** using different numbers of roots.

# roots	CASSCF (cm^{-1})		NEVPT2 (cm^{-1})	
	Effective[a]	2PT[b]	Effective[a]	2PT[b]
10	5.39	6.12	3.44	3.68
30	5.57	6.33	3.46	3.67
|difference|	0.18	0.21	0.02	0.01

[a] Values from effective Hamiltonian. [b]Values from 2nd order perturbation theory.

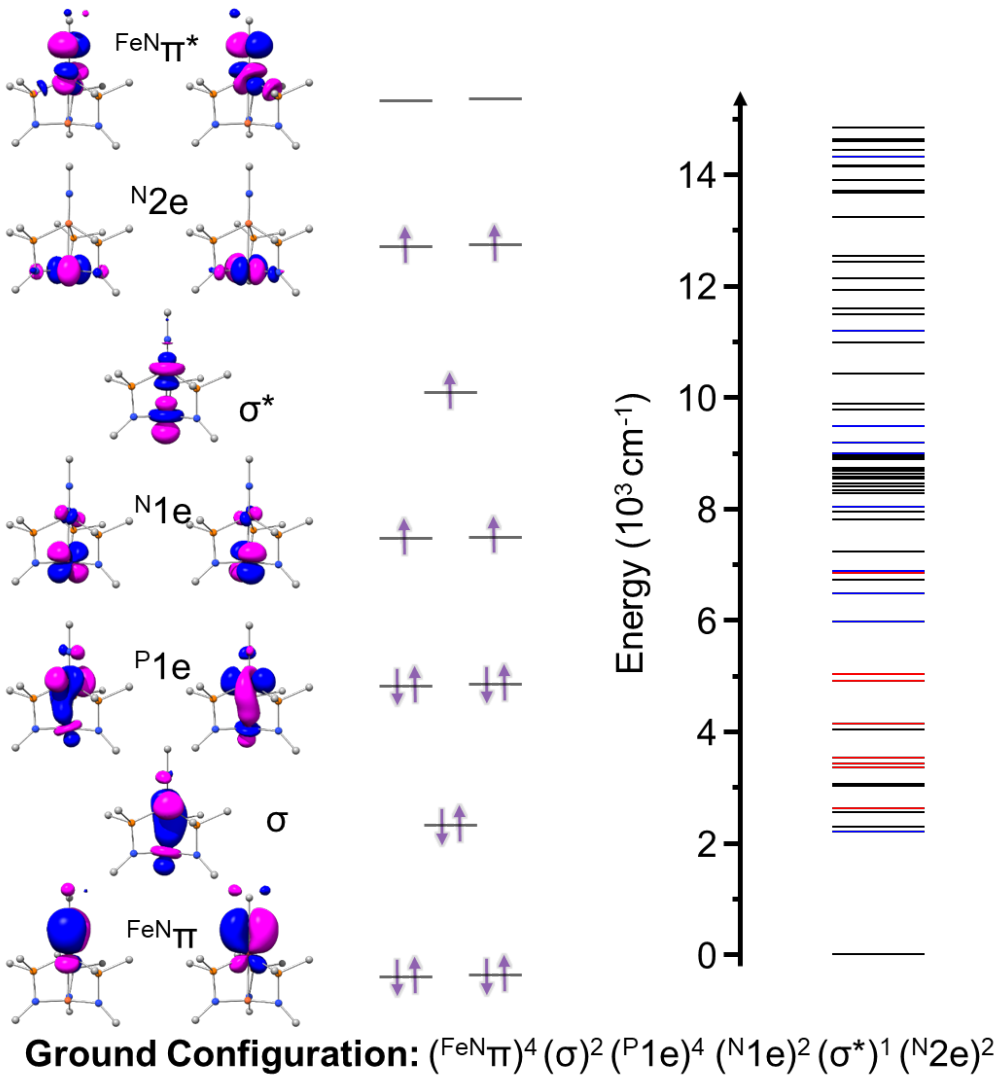

Figure S11. (Left) Qualitative MO diagram for **3** resulting from a SA-CASSCF/NEVPT2 calculation depicting the dominant configuration of the ground state. (Right) Low lying excited state energies where the ground state is labeled with the dominant configuration. The lines representing the energies of the states are colored according to their contribution to *D*: positive (red), negative (blue), and negligible/zero (black).

As described in the main text, the states in **3** are much less clear and do not lend themselves to simple assignments as in the case of **2**. We include the depiction of the SA-CASSCF orbitals as well as the spectrum of low-lying excited states in Figure S11.

Example Input Files Quantum Chemical Calculation

Quadrupole Splitting, Isomer Shift

```
! BP86 def2-TZVP TightSCF Grid5 NoFinalGrid SOMF(1x) SlowConv autoaux
%basis
newgto Fe "CP(PPP)" end
newauxgto Fe "autoaux" end
newgto h "def2-SVP" end
newauxgto h "autoaux" end
newgto c "def2-SVP" end
newauxgto c "autoaux" end
end

%method SpecialGridAtoms 26
SpecialGridIntAcc 7
end

* xyz 0 8
Geometry Coordinates
*
%eprnmr
  nuclei = all Fe {aiso, adip,aorb,fgrad, rho}
  gtensor  true
  printlevel          3
  Dtensor  ssandso
  DSOC    cp
  DSS      uno
  Ori      0
 end
```

CASSCF/NEVPT2 Calculations

```
! dkh dkh-def2-TZVP autoaux
%basis
newgto h "dkh-def2-SVP" end
newauxgto h "autoaux" end
newgto c "dkh-def2-SVP" end
newauxgto c "autoaux" end
end

%casscf
nel 13
norb 10
mult 8,6
nroots 10,10
trafostep RI
nevpt2 true
rel
dosoc true
gtensor true
end
end

* xyz 0 8
Geometry Coordinates
*
```

*xyz Coordinates for Optimized Truncated Model of **2** Used In CASSCF/Dimer Model Calculations*

Fe	0.00027053270821	0.00742967345374	-0.01607856043279
Fe	-0.00090803566830	0.00104055368742	2.42751388553046
P	1.09882154195225	1.85575255699632	0.85218323384500
P	0.00798752532143	0.01485603727300	-2.34009822870063
N	0.80742092441467	1.80869394172783	2.48980901810752
C	1.65105512302330	0.12025590111327	-3.18181350252613
H	1.55594333073351	0.09415015669003	-4.28756585303077
H	2.28939619798049	-0.72248029516895	-2.85303365537148
H	2.15464368806044	1.06133946716910	-2.88655737549765
C	-0.89654287903813	1.38601084153651	-3.18938534411198
H	-0.81648756115478	1.31603680941033	-4.29446609134005
H	-0.48698972930858	2.35980559342234	-2.85765188450689
H	-1.96588632495823	1.35341160765402	-2.90325904779315
C	-0.71960397225663	-1.45367889105049	-3.19628302015949
H	-0.68993406672298	-1.34870971451925	-4.30099754555811
H	-1.77023368596748	-1.58670374195248	-2.87304848200076
H	-0.15828871854629	-2.36300263853079	-2.90582593549833
P	-2.15287741077491	0.02939394818209	0.84410653591621
N	-1.97058715990440	-0.20454740808296	2.48151794091378
P	1.05282324235455	-1.87320836953600	0.84218045760475
N	1.16468100745783	-1.60017193778070	2.47980358262136
C	2.74060106528366	-2.34011934060049	0.21887543997381
H	3.17821230841269	-3.16834694693154	0.81436176320593
H	2.67654850275710	-2.66526644316997	-0.83961590561569
H	3.41427492472718	-1.46400067775048	0.28055634489766
C	0.18587364618363	-3.49411196537050	0.57753877153088
H	0.10843150715876	-3.72085104330362	-0.50483232237676
H	0.72170760646133	-4.32907912008966	1.07534503960584
H	-0.83530685523007	-3.42584166041050	1.00002240284060
C	1.58843568875731	-2.58414238433250	3.45983756618997
H	0.85320258637227	-3.41329551032097	3.60611357465435
H	2.56573292016735	-3.05922858058107	3.20207117535583
H	1.72501066644635	-2.10066461172399	4.45034023554351
C	1.44989765663093	2.66107758056546	3.47407839817386
H	2.53900477644952	2.44655667435877	3.60568646680451
H	1.36021840090251	3.74743190831365	3.23131925377120
H	0.97462859152858	2.52008660698946	4.46785032969238
C	-3.03340669078139	-0.08028261516772	3.46306404598794
H	-3.39173997300738	0.96947856936792	3.60084216536808
H	-3.92888500682343	-0.69866646562539	3.21266062244576
H	-2.67723111337481	-0.42874357732534	4.45562361435953
C	-3.39631864796384	-1.20281913276702	0.21963599986054
H	-4.33537645357308	-1.16727237649157	0.81020262678565
H	-3.64097181076222	-0.98937721672536	-0.84089108269201
H	-2.97285899110262	-2.22326592706792	0.28671724446074
C	-3.12786625807674	1.58769570405689	0.58026421763593
H	-3.28770887817404	1.76631910935043	-0.50218213009346
H	-4.11785885481514	1.53956719717743	1.07966382998960
H	-2.55956151067482	2.44005982249435	1.00063737356190
C	0.65343144469685	3.55132624702819	0.23410449104862
H	1.15311645132044	4.34462913008983	0.82816191875994
H	0.96099635398091	3.66116011684235	-0.82589040323709
H	-0.44215909432480	3.69352516751509	0.30103329469094
C	2.93530317853747	1.92065679298842	0.58570060344403
H	3.16780107476380	1.97435040744866	-0.49692553400871
H	3.38959874700957	2.79970066410299	1.08835351332629
H	3.38901847043020	1.00008980537130	1.00093492604701

*xyz Coordinates For The Optimized Truncated Model of **3** Used In CASSCF Calculations*

Fe	-0.02989838444308	-0.04745793557219	-1.44520391279206
Fe	0.01729817903259	0.03326870960058	1.10460138421312
P	1.73871464261916	1.01939781542569	0.11466397352131
P	0.01581405997979	-2.00997479914540	0.24119854385202
P	-1.74982373174678	1.00313100915756	0.17711459412078
N	1.53180581884495	1.15607657727572	-1.52843543398314
N	0.23081948058741	-2.00284638365732	-1.40631478064844
N	-1.85290808522667	0.70732615918112	-1.45483982470231
N	0.04886087379695	0.09023111714280	2.74674915003672
C	-1.51070717854070	-2.97737548168066	0.63273873797712
H	-1.69370257063201	-2.96968715130146	1.72478794769771
H	-2.37445882068816	-2.51279690873294	0.11979430253779
H	-1.41546075136744	-4.02849258044230	0.28949729546753
C	1.29610657304471	-3.10310720356985	1.00575732819617
H	2.29834977836998	-2.65702322603096	0.87173951170865
H	1.09538526185859	-3.20206221179553	2.09055414328721
H	1.28223271307880	-4.10992501459425	0.53915764127136
C	0.04683337725568	-3.14423607588281	-2.28489637336085
H	0.35596898604902	-2.88119671123906	-3.31837738884574
H	0.66535700207244	-4.02264795939608	-1.98179301998245
H	-1.01236055462360	-3.49434939180612	-2.34404086231198
C	-3.33685916113484	0.49362357775943	0.97729464951116
H	-3.44894012729606	-0.60450307863468	0.92141012264100
H	-3.32471484140185	0.79324410049874	2.04366683041290
H	-4.20172976820169	0.97278852952822	0.47326500802121
C	-2.73971545185958	1.39080366042936	-2.37966581883239
H	-2.67738967492207	0.91992179045505	-3.38327758780624
H	-3.81005223728484	1.33462760196974	-2.06786745836661
H	-2.49430875571967	2.47226406541105	-2.51456034957365
C	-1.81973325581027	2.83030361564666	0.44994250646925
H	-1.71959172419260	3.05641941765086	1.52916420147826
H	-0.98474037999711	3.30816909786874	-0.09666103780229
H	-2.77705080515967	3.25143248156045	0.07889619144025
C	0.08026382794959	0.14798846503966	4.16514912777043
H	0.98065946595562	0.69409802161157	4.53704185232881
H	-0.81584641963564	0.67175589744217	4.57730877805183
H	0.10293596843927	-0.87189220130286	4.61960108232925
C	3.35733119115762	0.18546788754275	0.43642623303029
H	4.20038797126242	0.78229372459302	0.03060207358352
H	3.50333906112231	0.04897078456027	1.52550454314797
H	3.35541766211116	-0.80664311787238	-0.05381567570794
C	2.09312277275387	2.69513413908845	0.81117332260106
H	1.19987385489638	3.33847740039517	0.71203708567380
H	2.34417525266669	2.60228897914745	1.88606236642545
H	2.94261028490199	3.17005968114443	0.27771597702320
C	2.56569817104033	1.53158049968491	-2.47648747024140
H	3.38220007235895	0.77458991126854	-2.56830700029138
H	2.12663444376061	1.65373815583756	-3.48899203698936
H	3.04897093291744	2.50460455873912	-2.21985247358887